



## Research paper

## Discovery of novel anti-angiogenesis agents. Part 10: Multi-target inhibitors of VEGFR-2, Tie-2 and EphB4 incorporated with 1,2,3-triazol

Xiaoyan Pan, Liyuan Liang, Ru Si, Jin Wang, Qingqing Zhang, Huaxin Zhou, Lin Zhang, Jie Zhang\*

School of Pharmacy, Health Science Center, Xi'an Jiaotong University, Xi'an, 710061, China

## ARTICLE INFO

## Article history:

Received 18 September 2018  
 Received in revised form  
 25 October 2018  
 Accepted 17 November 2018  
 Available online 22 November 2018

## Keywords:

Anti-angiogenic agents  
 Multi-target  
 Triple RTK inhibitors  
 DFG-binding group  
 1,2,3-Triazole

## ABSTRACT

VEGFR-2, Tie-2, and EphB4 are essential for both angiogenesis and tumorigenesis. Herein, we developed a series of pyridines incorporated with 1,2,3-triazole as multi-target inhibitors based on the crystal structure alignment of the kinase domain of angiogenic RTKs. Biological results indicated that these multi-target inhibitors displayed considerable potential as novel anti-angiogenic agents. Among them, compound **BD7** exhibited the most potent inhibition against the three RTKs simultaneously, and good activity on inhibiting viability of human umbilical endothelial cells. Therefore, 1,2,3-triazole could serve as a promising DFG binding group for multi-target inhibitors of VEGFR-2, Tie-2 and EphB4 bearing pyridine as hinge binding group.

© 2018 Elsevier Masson SAS. All rights reserved.

## 1. Introduction

Angiogenesis plays a critical role in the pathogenesis of a variety of disorders including cancer, proliferative retinopathies, rheumatoid arthritis or psoriasis, and it has been identified as a crucial factor in metastasis, which is a major factor leading to cancer-related death [1]. Thus, anti-angiogenesis has been considered as a valid strategy for tumor therapy, and many efforts have been focused on developing angiogenesis inhibitors. In the past decades, numbers of pro-angiogenic factors such as VEGFR-2, FGFR, PDGFR, Tie-2 and EphB4, also known as receptor tyrosine kinases (RTKs), have been identified as potential targets for angiogenesis inhibitors [2]. However, it's a known fact that many anti-angiogenic agents have failed in clinic trials. Even though some angiogenesis inhibitors have been approved for clinical use, many problems have been occurred including resistance, enhancing hypoxia, and reducing delivery of drugs. The main reason is the compensatory activation of multiple RTKs [3]. Meanwhile, cancer cells secrete various RTKs involved in the process of angiogenesis [4]. Therefore, simultaneous inhibition and combinatorial targeting of multiple pro-angiogenic RTKs

have been applied as valuable strategy to promote anti-angiogenesis therapy.

VEGFR-2, Tie-2, EphB4, highly expressed in endothelial cells (ECs), have been indicated to play an essential role in both vasculogenesis and angiogenesis [5]. VEGFR-2 mainly contributes to very early steps of angiogenesis including ECs survival, proliferation and migration, while TIE2 and EphB4 contribute to later step including vessel stabilization, maturation, remodeling of vasculature, and vascular development [6–9]. Furthermore, these three RTKs have been confirmed to be significant in tumor development and prognosis [10]. To the best of our knowledge, these three RTKs contain a high conserved catalytic site binding with ATP, and their catalytic domains and ATP-binding site are quite similar [11,12]. Overlay of crystal structures of the three RTKs is depicted in Fig. 1, which shows no significant difference among each other with RMSD value 0.849 Å, 0.725 Å and 0.706 Å respectively. Therefore, VEGFR-2, TIE-2 and EphB4 are chose as targets for developing multi-targeted anti-angiogenesis agents.

In our former work, our interest was in discovery of novel VEGFR-2 inhibitors as anti-angiogenesis agents. Along this line, with natural alkaloid taspine as the lead compound, rounds of structure optimization were performed to develop novel VEGFR-2 inhibitors [13–15]. Among them, BPS-7, biphenyl-aryl urea incorporated with salicylal-doxime, has been developed as potent VEGFR-2 inhibitor. It significantly inhibited the proliferation of

\* Corresponding author.

E-mail address: [zhj8623@mail.xjtu.edu.cn](mailto:zhj8623@mail.xjtu.edu.cn) (J. Zhang).

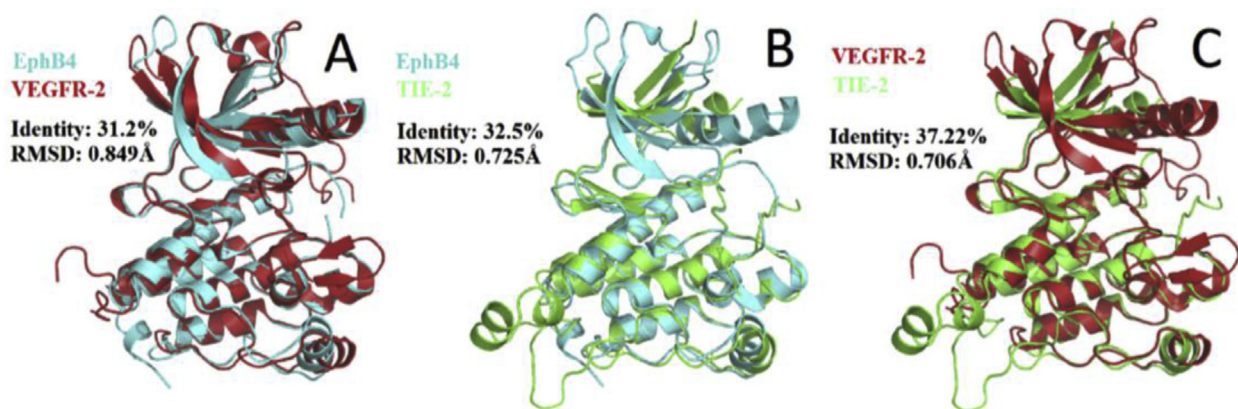


**Fig. 1.** Protein structure alignment of three angiogenic RTKs to each other (VEGFR-2: Red, TIE-2: Green, and EphB4: Cyan). (For interpretation of the references to colour in this figure legend, the reader is referred to the Web version of this article.)

human umbilical vein endothelial cells, and also effectively inhibited blood vessel formation in a tissue model for angiogenesis. Further mechanism study revealed that this compound displayed selective inhibition against TIE-2 and EphB4 besides VEGFR-2 [16], making the design of multiple kinase inhibitors feasible. Based on above findings, **BPS-7** was used as leading compound in our continued work for developing novel multiple RTKs inhibitors as anti-angiogenesis agents.

By doing interaction analysis of **BPS-7** with RTKs, we dissected the lead into four regions as shown in Fig. 2 for optimization work. Based on this model, various modification targeting hinge binding group (HBG), crucial for inhibitors' affinity, has been performed to discover original chemotypes. As is known, urea unit, interacting with DFG-motif, is another key part for kinase inhibitors' binding, thus optimization of DFG-motif interacting group is imperative. Therefore, the work described here is focused on modification of group interacting with DFG-motif. Inspired by bioisosteric paradigm, urea moiety was replaced with 1,2,3-triazole which may bears more hydrogen bond donors and acceptors, providing novel scaffold for multiple RTKs inhibitors. In addition, other three parts were also modified according to our previous work, exploring triple kinase inhibitors with novel scaffold. First, pyridine and 2-methoxy pyridine was incorporated as new HBG of multiple inhibitors, supposing that it might simultaneously form hydrogen bonds with hinge of three RTKs to improve affinity toward three targets. Second, the two methoxyl groups on biphenyl of **BSP-7** were removed to reduce the steric hindrance of inhibitors when binding with receptors. Third, various anilines were incorporated as they are beneficial for anti-tumor potency and could enhance the persistence [17].

Encouraged by previous results, we proposed that multiple RTKs-inhibition could afford novel anti-angiogenic agents. Herein, we performed the design, synthesis and biological evaluation of pyridine series compounds. Several pyridine derivatives incorporated with 1,2,3-triazole displayed promising anti-angiogenic potency. The representative compound **BD-7** could be considered as a promising lead compound for further structural optimization.

## 2. Results and discussion

### 2.1. Chemistry

The synthetic route of title compounds was illustrated in Scheme 1. Firstly, the key intermediates **4** were prepared in a two-step sequence from commercially available 1-bromo-4-(bromomethyl) benzene (**2**). 1-bromo-4-(bromomethyl) benzene (**2**) was converted to 1-(azidomethyl)-4-bromo-benzene (**3**) with sodium azide as azide reagent [18]. Then, various substituted phenylacetylenes (**1**) was reacted with intermediate (**3**) by click reaction in mixture of ethanol and water to generate corresponding triazole derivatives (**4**) [19]. Subsequently, the title compounds (**BD1-BD7**) were prepared from key intermediates (**4**) and commercial (6-methoxypyridin-3-yl)boronic acid (**5**) by Pd-catalyzed Suzuki coupling [20], while the other title compounds (**BD9-BD16**) were obtained from key intermediates (**4**) and commercial pyridin-3-ylboronic acid (**6**) using the same method. In addition, cyclopropanecarbonyl chloride coupling of (**BD7**) through the acylation reaction afford the title compound (**BD8**). All the target compounds were characterized by Mass spectrum (MS),  $^1\text{H}$  NMR,  $^{13}\text{C}$  NMR, and melting point analysis (Supplementary Material).

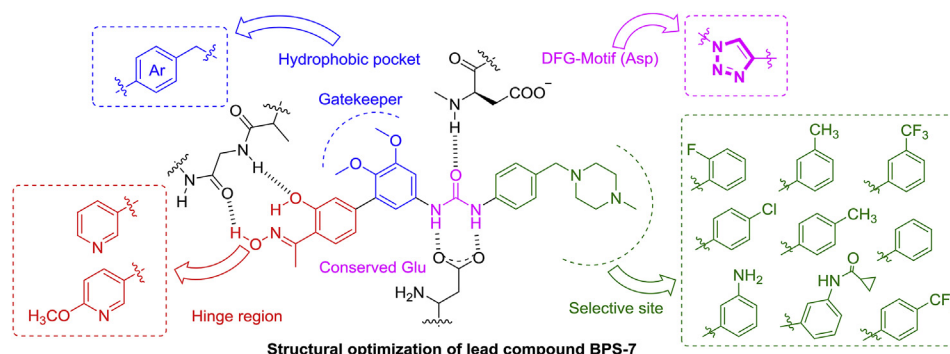
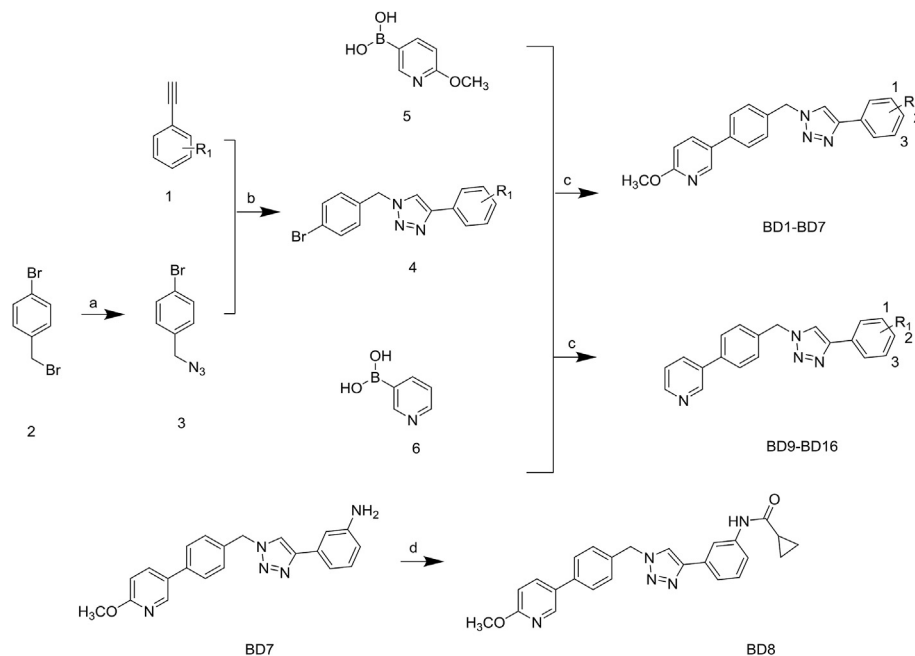


**Fig. 2.** Design strategy and structures of novel multi-target anti-angiogenic agents.



**Scheme 1.** Synthesis Route of Pyridine Series Compounds (**BD1-BD16**)

*Reagents and conditions* (a) NaN<sub>3</sub>, DMF, rt, 12 h; (b) *L*-sodium ascorbate, copper sulfate pentahydrate, ethanol, H<sub>2</sub>O, rt; (c) dioxane, H<sub>2</sub>O, Pd(PPhF)<sub>2</sub>, K<sub>2</sub>CO<sub>3</sub>, reflux; (d) 0 °C, CH<sub>2</sub>Cl<sub>2</sub>, triethylamine, 30min, cyclopropyl carbonyl chloride, rt.

## 2.2. Biology assays

In order to evaluate the biological activities of title compounds as anti-angiogenic agents, we firstly tested the enzymatic inhibitory activity of the title compounds against three angiogenic RTKs, VEGFR-2, Tie-2, and EphB4. Subsequently, their inhibition on viability of HUVECs (EA.hy926) was evaluated to prove the anti-angiogenic potency. In parallel, a marketed multi-target RTK inhibitors, sorafenib, was used as positive control.

### 2.2.1. RTK inhibitory activities

All the title compounds were evaluated for their inhibitory potency against VEGFR-2, Tie-2 and EphB4 with sorafenib as positive control. Tyrosine kinase inhibition were tested by ADP-Glo™ assay [21]. As observed in Table 1, several compounds exhibited simultaneous inhibition against the three angiogenic RTKs. In particular, compound **BD7** displayed the most potent activity against VEGFR-2, Tie-2 and EphB4 with IC<sub>50</sub> values of 1.85 nM, 0.73 nM and 2.99 nM. For compounds with 2-methoxy pyridine as hinge binding group, besides compound **BD7**, compound **BD1** bearing fluorine substituents exhibited potent inhibitory activity against RTKs (VEGFR-2 IC<sub>50</sub> = 1.63 nM, Tie-2 IC<sub>50</sub> = 0.36 nM, and EphB4 IC<sub>50</sub> = 28.68 nM), while **BD6** with trifluoromethyl group showed better potency than other compounds. The results indicated that halogen substituent and trifluoromethyl were the most favorable for their enzymatic inhibitory activity. In addition, compound **BD8** was only potent toward VEGFR-2 compared with **BD7**, which suggested that cyclopropanoylation of terminal amino group was not beneficial for improving activity.

For title compounds with pyridine as hinge binding group, the majority of them exhibited poor activity except for compound **BD10** bearing fluorine substituent on terminal aniline. It exhibited moderate RTKs (VEGFR-2, Tie-2, and EphB4) inhibitory activities with IC<sub>50</sub> values of 300.42 nM, 61.26 nM, and 96.86 nM, respectively. These results indicated that methoxyl side chain on *ortho*-position of pyridine was favorable for their potency. Besides, for

**Table 1**

Structures and RTK inhibitory activities of title compounds (**BD1-BD16**) (IC<sub>50</sub>, nM).

Compounds	R <sub>1</sub>	R <sub>2</sub>	VEGFR-2	Tie-2	EphB4
BD1	1-Cl	OCH <sub>3</sub>	1.63	0.36	28.68
BD2	6-F	OCH <sub>3</sub>	>1000	ND	266.77
BD3	H	OCH <sub>3</sub>	10.56	>1000	>1000
BD4	2-CH <sub>3</sub>	OCH <sub>3</sub>	96.17	0.26	ND
BD5	1-CH <sub>3</sub>	OCH <sub>3</sub>	11.07	>1000	ND
BD6	2-CF <sub>3</sub>	OCH <sub>3</sub>	75.86	0.30	>1000
BD7	1-NH <sub>2</sub>	OCH <sub>3</sub>	1.85	0.73	2.99
BD8	H <sub>2</sub> N-C(=O)-Cyclopropyl	OCH <sub>3</sub>	0.52	ND	ND
BD9	1-Cl	H	668.70	0.28	ND
BD10	6-F	H	300.42	61.26	96.86
BD11	H	H	36.16	24.19	ND
BD12	2-CH <sub>3</sub>	H	15.90	>1000	0.44
BD13	1-CH <sub>3</sub>	H	1.33	0.45	>1000
BD14	2-CF <sub>3</sub>	H	ND	>1000	>1000
BD15	1-CF <sub>3</sub>	H	>1000	ND	>1000
BD16	1-NH <sub>2</sub>	H	ND	265.72	ND
<b>sorafenib</b>			0.17	0.39	0.22

ND=Not Determined.

these pyridines, amino or halogen substituent on terminal aniline were beneficial for RTK inhibitory activities. Since most compounds displayed moderate to high inhibition potency against VEGFR-2, Tie-2 and EphB4, it might conclude that 1,2,3-triazole could be considered as novel unit to replace urea unit for VEGFR-2/Tie-2/EphB4 inhibitors.

### 2.2.2. Cell growth inhibition against the human umbilical vein endothelial cells (EA.hy926) and cancer cells

In order to determine the potential anti-angiogenic effect of

**Table 2**  
Anti-proliferative activity of inhibitors against human vascular endothelial cell (IC<sub>50</sub>, μM).

Compound	EA.hy926	Compound	EA.hy926
BD1	439.89	BD9	431.19
BD2	708.14	BD10	9.28
BD3	110.17	BD11	12.09
BD4	677.69	BD12	6.49
BD5	43.94	BD13	134.15
BD6	121.97	BD14	170.47
BD7	14.49	BD15	136.53
BD8	ND	BD16	24.31
		<b>Sorafenib</b>	11.74

these multi-target inhibitors, we evaluate the inhibition of title compounds on HUVECs (EA.hy926) viability using cell counting kit-8 (CCK-8) method [22]. As depicted in Table 2, majority of title compounds displayed moderate to high anti-proliferative activities with IC<sub>50</sub> values ranging from 6.49 μM to 708.14 μM. Four compounds (**BD7**, **BD10**, **BD11** and **BD 12**) exhibited potent inhibition against the growth of human vascular endothelial cell with IC<sub>50</sub> values less than 20 μM. Particularly, compound **BD7** with the most potent RTK inhibitory activities exhibited high cell growth inhibition with IC<sub>50</sub> value (14.49 μM) comparable to that of positive control sorafenib (11.74 μM). This compound represents the promising candidate with a “triple” inhibition profile as well as anti-angiogenic potency. It might not only inhibit the process of angiogenesis, but also prevent the occurrence of resistance.

In order to investigate the potential anticancer potency of these multi-target RTK inhibitors, the most potent **BD7** was selected to examine its anti-proliferative activity against several cancer cells including human hepatic cancer cell lines (SMMC-7721), human breast cancer cell lines (MCF-7), human epidermoid carcinoma cell line (A431), human lung cancer cell (A549), human colon carcinoma cell line (LOVO), human pancreatic cancerous cell lines (PANC-1), and human cervical cancer cell line (HeLa). Highly consistent with the RTK inhibition, it was found that **BD7** exhibited potent anti-proliferative activity against various cancer cell lines with IC<sub>50</sub> values ranging from 0.07 μM to 0.49 μM (Table 3). In particular, it displayed the highest anticancer potency against human epidermoid carcinoma cell line (A431) and human colon carcinoma cell line (LOVO) with IC<sub>50</sub> values of 0.07 μM and 0.10 μM, respectively.

### 2.2.3. Molecular docking study

For further structural optimization and investigation of the potential binding mode, molecular modeling studies were performed using Sybyl-X (version 2.0, Tripos INC.St. Louis, MO). The most potent compound, **BD7**, was constructed and optimized using Powell's method with a Tripos force field. The molecular modeling was performed using Sybyl-X/Surflex-dock module, and the residues in 5.0 Å radius around the ligand of VEGFR-2 (PDB ID: 4ASD), TIE-2 (PDB ID: 2P4I) and EphB4 (PDB ID: 4BB4) were selected as the active site [23]. The binding mode of **BD7** with the ATP-pocket of VEGFR-2, Tie-2, EphB4 were depicted in Figs. 3–5.

As shown in Fig. 3, **BD7** was nicely bound to VEGFR-2 and

**Table 3**  
Anti-proliferative activities of title compound (BD7) against various cancer cells.

Compound	Cancer Cell Lines, IC <sub>50</sub> (μM)						
	SMMC-7721	MCF-7	A431	A549	LOVO	PANC-1	HeLa
BD7	0.24	0.35	0.07	0.18	0.10	0.49	0.29
Sorafenib	0.30	0.09	0.12	0.08	0.25	0.15	0.27

presented the similar binding conformation with sorafenib which was displayed as orange. The oxygen atom of methoxyl and nitrogen atom on pyridine ring formed two hydrogen bonds with Cys919 in the hinge region of VEGFR-2 with distance of 2.59 Å and 2.24 Å, respectively. The two nitrogen atoms on triazole ring formed two hydrogen bonds with conserved Asp1046 of DFG motif for the bond length of 2.68 Å and 1.95 Å, respectively. In addition, the NH<sub>2</sub> group on terminal phenyl ring, as hydrogen-bond donor, generated one hydrogen bond with Val899, and the bond length is 2.17 Å. Favorable binding interactions of **BD7** with the active site of Tie-2 was displayed in Fig. 4 with three hydrogen bonds as follows: 1) the first forming between N atom of pyridine ring and NH<sub>2</sub> of Ala905 in hinge region, the distance was 2.75 Å, 2) the second forming between N atom of triazole and NH<sub>2</sub> of Lys855 with the distance of 2.38 Å, 3) the third was observed between NH<sub>2</sub> group of terminal phenyl ring and C=O of Glu872 with bond length of 2.22 Å. As for EphB4, the preferred binding model was described in Fig. 5. The docking result suggested that **BD7** was fit well to the ATP pocket of EphB4 compared with its own ligand, and there are three hydrogen bonds between **BD7** and EphB4. First, the oxygen atom of methoxyl formed one hydrogen bond with Ser757, and the bond length was 2.66 Å. Second, between the nitrogen atom of pyridine ring and OH of Thr693, there was one hydrogen bond with distance of 2.44 Å. Moreover, one hydrogen bond was observed between NH<sub>2</sub> of terminal phenyl ring and C=O of Asn698, with distance of 2.00 Å.

Based on docking analysis above, compound **BD7** interacted well with VEGFR-2, TIE-2 and EphB4, and its interaction mode was similar as that of these three RTKs' ligands, which is quite consisted with its excellent RTKs inhibitory activity. For details, pyridine with methoxy sidechain, as expected, generated hydrogen bond with hinge region of all three RTKs, and could be considered as novel hinge-binding group for further study. 1,2,3-triazole ring interacted with DFG-motif of VEGFR-2 and TIE-2 through hydrogen bonding, but no interaction with EphB4, which may explained the lower activity of compound **BD7** against EphB4 compared with the other two RTKs. Furthermore, triazole position was highly overlapped with urea in VEGFR-2 ligand and amide in TIE-2 ligand, respectively. All of these suggested that our strategy of introducing triazole instead of urea unit was valid, providing novel scaffold for multi-target RTKs inhibitors. In addition, the amine group on terminal phenyl ring was beneficial for improving activity toward RTKs, making compound **BD7** the best one in this series inhibitors.

### 3. Conclusion

Herein, we described the triple inhibitors of VEGFR-2/Tie-2/EphB4 as potential anti-angiogenic agents. Since these RTKs play essential roles in angiogenesis. These multiple inhibitors might be potent to prevent the resistance of single-target drugs. 1,2,3-Triazole was firstly introduced to diaryl urea core as DFG-binding group while various pyridines as hinge-binding group. Finally, a series of pyridine derivatives incorporated with 1,2,3-triazole as multiple inhibitors were designed, synthesized, and evaluated. The biological results indicated that **BD7** displayed simultaneous inhibition of VEGFR-2, Tie-2, and EphB4. Meanwhile, it displayed the most potent anti-proliferative activity against human vascular endothelial cell (EA.hy926) comparable to sorafenib. Moreover, Molecular modeling revealed that these compounds could suppress VEGFR-2, Tie-2, and EphB4 kinase activity through preferential binding at the ATP-binding site. In conclusion, our results identified the rationality of design strategies of triple VEGFR-2/Tie-2/EphB4 inhibitors as novel anti-angiogenic agents. Among them, **BD7** could be considered as a promising starting point for further optimization of 1,2,3-triazole incorporated derivatives as VEGFR-2/Tie-2/EphB4 inhibitors.

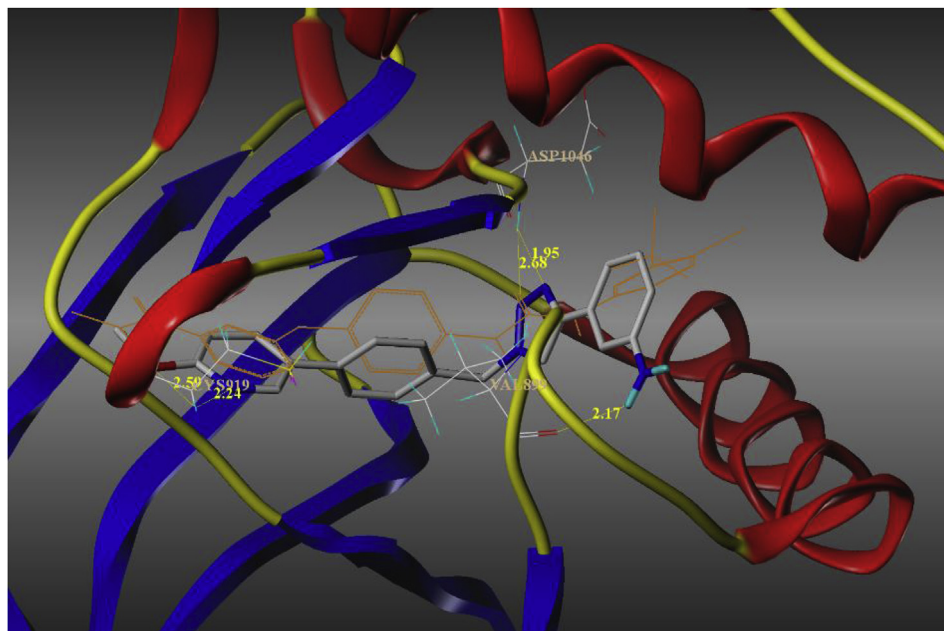


**Fig. 3.** Docked molecule (BD7) in the crystal structure of VEGFR-2 (PDB ID: 4ASD). Hydrogen bonds were depicted in dashed yellow lines. (For interpretation of the references to colour in this figure legend, the reader is referred to the Web version of this article.)

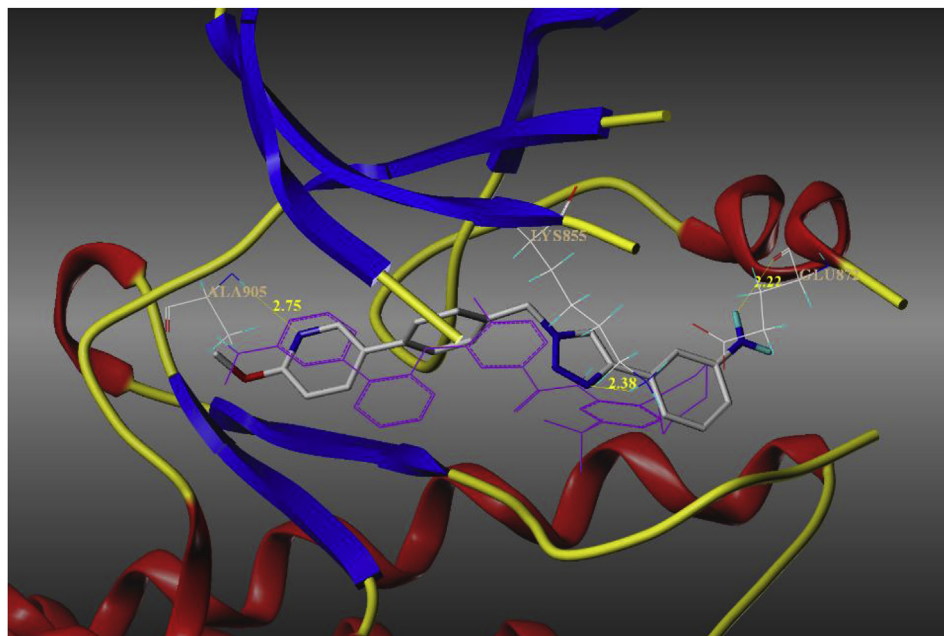


**Fig. 4.** Docked molecule (BD7) in the crystal structure of TIE-2 (PDB ID: 2P4I). Hydrogen bonds were depicted in dashed yellow lines. (For interpretation of the references to colour in this figure legend, the reader is referred to the Web version of this article.)

Our findings may contribute to the discovery of novel anti-angiogenic agents for the intervention of pathological angiogenesis-related diseases.

#### 4. Experimental section

##### 4.1. Chemistry: general procedure

All reagents were purchased from commercial suppliers and purified according to the standard procedure. The reaction except those in aqueous media are carried out by standard techniques for

the exclusion of moisture. Reaction progress was monitored by thin layer chromatography (TLC) on 0.25-mm silica gel plates (GF254) and visualized with UV. Column chromatography was performed with silica gel (300–400 mesh). Melting points were determined using an electrothermal melting point apparatus and were uncorrected.  $^1\text{H}$  NMR and  $^{13}\text{C}$  NMR spectra were measured at 400 MHz on a Bruker Advance AC400 instrument with TMS as an internal standard. Mass spectra were obtained on a Shimadzu HPLC-MS-QP2010 instrument.

General procedure for the synthesis of pyridine series compounds BD1–BD16.

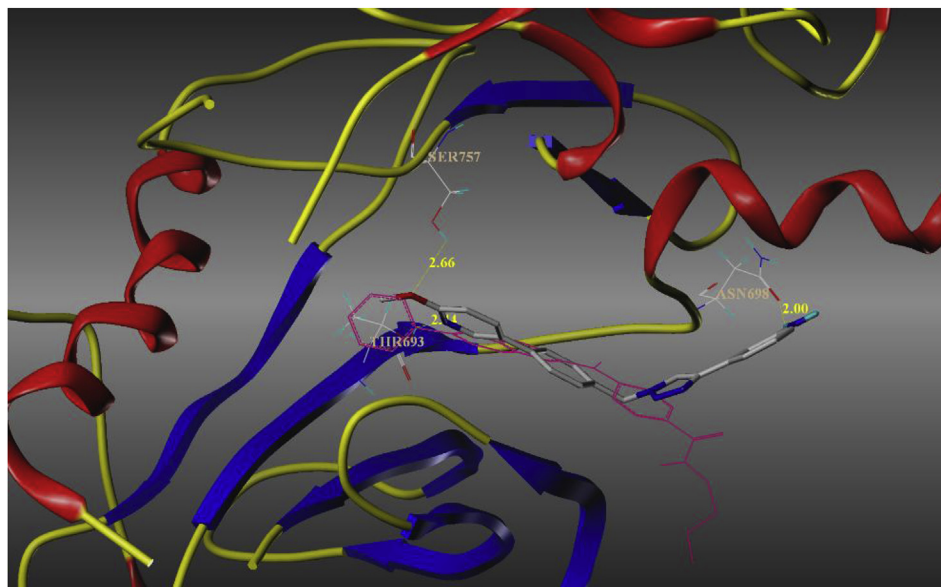


**Fig. 5.** Docked molecule (**BD7**) in the crystal structure of EphB4 (PDB ID: 4BB4). Hydrogen bonds were depicted in dashed yellow lines. (For interpretation of the references to colour in this figure legend, the reader is referred to the Web version of this article.)

#### 4.1.1. 1-(azidomethyl)-4-bromobenzene (**3**)

1-bromo-4-(bromomethyl)benzene (2.00 g 8.00 mmol) was dissolved in anhydrous DMF on ice-bath, 0.78 g (11.99 mmol) of sodium azide dissolved in water was added into the mixture. Stirring was continued for 10 min, and sodium azide (0.78 g, 11.99 mmol) dissolved in water was added dropwise to above mixture again at room temperature. After stirring at room temperature overnight. The reaction solution was extracted with EtOAc (60 mL  $\times$  3). The organic layer was washed with water and brine (40 mL  $\times$  3), and dried over  $\text{Na}_2\text{SO}_4$ . After filtration and concentration *in vacuo*, the residue was purified by silica gel flash chromatography (PE/ AcOEt = 40:1) to afford (**3**) as a slight yellow oil (1.45 g 85.1%).

#### 4.1.2. 1-(4-bromobenzyl)-4-(3-chlorophenyl)-1H-1,2,3-triazole (**4**)

A flask charged with 1-(azidomethyl)-4-bromobenzene (**3**) (1.20 g 5.63 mmol), 1-chloro-3-ethynyl-benzene (0.78 g 5.63 mmol) was dissolved in anhydrous ethanol (30 mL). L-sodium ascorbate (0.45 g 2.25 mmol), copper sulfate pentahydrate (0.29 g 1.13 mmol) and water (3 mL) were then added into the mixture. Stirring was performed at room temperature overnight. After filtration and concentration *in vacuo*, the residue was purified by silica gel flash chromatography (PE/AcOEt = 3:1) affording (**4**) as white solid (1.31 g, 66.7%).

#### 4.1.3. 5-(4-((4-(3-chlorophenyl)-1H-1,2,3-triazol-1-yl) methyl) phenyl)-2-methoxypyridine (**BD1**)

A flask charged with Pd(dppf) $\text{Cl}_2$  (0.25 g, 0.34 mmol),  $\text{K}_2\text{CO}_3$  (1.43 g, 10.35 mmol), 1-(4-bromobenzyl)-4-(3-chlorophenyl)-1H-1,2,3-triazole (**4**) (1.20 g 3.44 mmol) and (6-methoxy-pyridin-3-yl) boronic acid (**5**) (0.68 g, 4.47 mmol), were flushed with nitrogen and suspended in 1,4-dioxane (30 mL) and water (10 mL). The mixture was then refluxed overnight under nitrogen. The hot suspension was filtered, and the filtrate was distilled by rotary evaporation to remove 1,4-dioxane. Water (50 mL) was added and the solution was extracted with EtOAc (60 mL  $\times$  3). The combined EtOAc layer was washed with water, and dried over  $\text{Na}_2\text{SO}_4$ . After filtration and concentration *in vacuo*, the residue was purified by silica gel flash chromatography (PE/AcOEt = 15:1) affording (**BD1**) as white solid (0.39 g, 30%). Mp. = 160–162 °C. MS (EI)  $[M]^+$ :  $m/z$  = 376.  $^1\text{H}$  NMR

(400 MHz,  $\text{DMSO}-d_6$ )  $\delta$  10.87 (s, 1H), 9.21 (s, 1H), 8.99 (s, 1H), 8.63 (d,  $J$  = 2.2 Hz, 1H), 8.14 (d,  $J$  = 8.7 Hz, 2H), 8.04 (m,  $J$  = 8.7, 2.4 Hz, 1H), 7.65 (t,  $J$  = 8.3 Hz, 4H), 7.58 (d,  $J$  = 8.7 Hz, 2H), 2.03 (t,  $J$  = 12.3, 8.6, 4.8 Hz, 1H), 0.92–0.71 (m, 4H).  $^{13}\text{C}$  NMR (101 MHz,  $\text{DMSO}-d_6$ )  $\delta$  163.62, 145.82, 145.20, 138.01, 137.39, 135.35, 134.15, 133.20, 131.34, 129.21, 129.15, 128.14, 127.20, 125.22, 124.12, 122.80, 111.09, 53.74, 53.25.

The compound **BD2–BD16** were prepared using the same procedure described above.

#### 4.1.4. 5-(4-((4-(2-fluorophenyl)-1H-1,2,3-triazol-1-yl) methyl) phenyl)-2-methoxypyridine (**BD2**)

Mp. = 122–124 °C. MS (EI)  $[M]^+$ :  $m/z$  = 360.  $^1\text{H}$  NMR (400 MHz,  $\text{DMSO}-d_6$ )  $\delta$  8.16 (t,  $J$  = 7.7 Hz, 1H), 8.02 (dd,  $J$  = 8.7, 2.6 Hz, 1H), 7.70 (d,  $J$  = 8.2 Hz, 2H), 7.49 (d,  $J$  = 8.2 Hz, 1H), 7.45–7.31 (m, 3H), 6.93 (d,  $J$  = 8.6 Hz, 1H), 5.76 (s, 2H), 3.91 (s, 3H).  $^{13}\text{C}$  NMR (101 MHz,  $\text{DMSO}-d_6$ )  $\delta$  163.67, 160.20, 157.75, 145.26, 140.45, 138.06, 137.39, 135.64, 130.25, 130.17, 129.22, 127.84, 127.80, 127.23, 125.51, 125.47, 124.56, 124.45, 118.89, 118.76, 116.64, 116.43, 111.13, 53.79, 53.08.

#### 4.1.5. 2-methoxy-5-(4-((4-phenyl-1H-1,2,3-triazol-1-yl) methyl) phenyl)pyridine (**BD3**)

Mp. = 196–197 °C. MS (EI)  $[M]^+$ :  $m/z$  = 342.  $^1\text{H}$  NMR (400 MHz,  $\text{DMSO}-d_6$ )  $\delta$  8.69 (s, 1H), 8.48 (d,  $J$  = 2.3 Hz, 1H), 8.01 (d,  $J$  = 11.1 Hz, 1H), 7.86 (d,  $J$  = 7.4 Hz, 2H), 7.69 (d,  $J$  = 8.1 Hz, 2H), 7.45 (t,  $J$  = 7.5 Hz, 4H), 7.34 (d,  $J$  = 7.3 Hz, 1H), 6.91 (d,  $J$  = 8.6 Hz, 1H), 5.70 (s, 2H), 3.89 (s, 3H).  $^{13}\text{C}$  NMR (101 MHz,  $\text{DMSO}-d_6$ )  $\delta$  163.64, 147.18, 145.22, 138.04, 137.35, 135.60, 131.13, 129.39, 129.20, 129.14, 128.39, 127.21, 125.64, 122.06, 111.12, 53.77, 53.17.

#### 4.1.6. 2-methoxy-5-(4-((4-(*p*-tolyl)-1H-1,2,3-triazol-1-yl) methyl) phenyl)pyridine (**BD4**)

Mp. = 168–170 °C. MS (EI)  $[M]^+$ :  $m/z$  = 356.  $^1\text{H}$  NMR (400 MHz,  $\text{DMSO}-d_6$ )  $\delta$  8.62 (s, 1H), 8.48 (s, 1H), 8.01 (d,  $J$  = 8.6 Hz, 1H), 7.74 (d,  $J$  = 8.0 Hz, 2H), 7.69 (d,  $J$  = 8.1 Hz, 2H), 7.45 (d,  $J$  = 8.1 Hz, 2H), 7.25 (d,  $J$  = 7.9 Hz, 2H), 6.91 (d,  $J$  = 8.6 Hz, 1H), 5.68 (s, 2H), 3.89 (s, 3H), 2.33 (s, 3H).  $^{13}\text{C}$  NMR (101 MHz,  $\text{DMSO}-d_6$ )  $\delta$  163.67, 147.28, 145.25, 138.06, 137.71, 137.38, 135.65, 129.96, 129.24, 129.18, 128.40, 127.24, 125.61, 121.65, 111.14, 53.79, 53.17, 21.34.

#### 4.1.7. 2-methoxy-5-(4-((4-(*m*-tolyl)-1*H*-1,2,3-triazol-1-yl) methyl) phenyl)pyridine (**BD5**)

Mp. = 158–160 °C. MS (EI)  $[M]^+$ :  $m/z$  = 356. <sup>1</sup>H NMR (400 MHz, DMSO-*d*<sub>6</sub>) δ 8.65 (s, 1H), 8.49 (s, 1H), 8.01 (dd,  $J$  = 8.7, 2.6 Hz, 1H), 7.69 (d,  $J$  = 8.2 Hz, 3H), 7.65 (d,  $J$  = 7.8 Hz, 1H), 7.48–7.43 (m, 2H), 7.33 (t,  $J$  = 7.6 Hz, 1H), 7.15 (d,  $J$  = 7.7 Hz, 1H), 6.92 (d,  $J$  = 8.6 Hz, 1H), 5.69 (s, 2H), 3.89 (s, 3H), 2.35 (s, 3H). <sup>13</sup>C NMR (101 MHz, DMSO-*d*<sub>6</sub>) δ 163.68, 147.31, 145.26, 138.56, 138.07, 137.39, 135.62, 131.08, 129.32, 129.24, 129.21, 129.06, 127.25, 126.24, 122.83, 122.01, 111.15, 53.80, 53.20, 21.55.

#### 4.1.8. 2-methoxy-5-(4-((4-(4-(trifluoromethyl)phenyl)-1*H*-1,2,3-triazol-1-yl)methyl)phenyl) pyridine (**BD6**)

Mp. = 163–165 °C. MS (EI)  $[M]^+$ :  $m/z$  = 410. <sup>1</sup>H NMR (400 MHz, DMSO-*d*<sub>6</sub>) δ 8.87 (s, 1H), 8.49 (d,  $J$  = 2.2 Hz, 1H), 8.09 (d,  $J$  = 8.1 Hz, 2H), 8.01 (dd,  $J$  = 8.6, 2.6 Hz, 1H), 7.82 (d,  $J$  = 8.3 Hz, 2H), 7.70 (d,  $J$  = 8.2 Hz, 2H), 7.47 (d,  $J$  = 8.2 Hz, 2H), 6.92 (d,  $J$  = 8.6 Hz, 1H), 5.73 (s, 2H), 3.89 (s, 3H). <sup>13</sup>C NMR (101 MHz, DMSO-*d*<sub>6</sub>) δ 163.68, 145.84, 145.27, 138.06, 137.47, 135.40, 135.13, 129.27, 129.21, 127.27, 126.44, 126.40, 126.21, 123.38, 111.15, 53.79, 53.34.

#### 4.1.9. 3-(1-(4-(6-methoxypyridin-3-yl)benzyl)-1*H*-1,2,3-triazol-4-yl)aniline (**BD7**)

Mp. = 156–158 °C. MS (EI)  $[M]^+$ :  $m/z$  = 357. <sup>1</sup>H NMR (400 MHz, DMSO-*d*<sub>6</sub>) δ 8.49 (d,  $J$  = 2.4 Hz, 1H), 8.02 (dd,  $J$  = 8.7, 2.6 Hz, 1H), 7.70 (d,  $J$  = 8.2 Hz, 1H), 7.46 (d,  $J$  = 8.2 Hz, 2H), 7.15–7.05 (m, 2H), 6.98–6.89 (m, 2H), 6.54 (d,  $J$  = 7.9 Hz, 1H), 5.68 (s, 2H), 5.19 (s, 2H), 3.90 (s, 3H). <sup>13</sup>C NMR (101 MHz, DMSO-*d*<sub>6</sub>) δ 163.66, 149.57, 147.88, 145.25, 138.06, 137.35, 135.73, 131.61, 129.86, 129.25, 129.17, 127.22, 121.62, 114.11, 113.51, 111.13, 110.94, 53.79, 53.10.

#### 4.1.10. *N*-(4-(1-(4-(6-methoxypyridin-3-yl)benzyl)-1*H*-1,2,3-triazol-4-yl)phenyl) cyclopropanecarboxamide (**BD8**)

3-(1-(4-(6-methoxypyridin-3-yl)benzyl)-1*H*-1,2,3-triazol-4-yl) aniline (**BD7**) (0.20 g, 0.56 mmol) was dissolved in anhydrous CH<sub>2</sub>Cl<sub>2</sub> (10 mL), and the mixture was stirred on the ice-bath for 10 min. Triethanolamine (0.14 mL, 1.01 mmol) diluted with CH<sub>2</sub>Cl<sub>2</sub> (2 mL) was then added into the mixture. Stirring was continued for 30 min, a solution of cyclopropanecarbonyl chloride (0.11 mL, 1.12 mmol) in anhydrous CH<sub>2</sub>Cl<sub>2</sub> was added dropwise to the above mixture. Then, the ice bath was removed, and the mixture was reacted at room temperature overnight. The reaction solution was diluted with water (10 mL), and extracted with CH<sub>2</sub>Cl<sub>2</sub> (30 mL × 3). The combined organic layer was washed with water (20 mL × 2) and brine, and dried over Na<sub>2</sub>SO<sub>4</sub>. After filtration and concentration *in vacuo*, the residues was purified by silica gel flash chromatography (PE/AcOEt = 15:1) to afford (**BD8**) as white solid (0.19 g, 80%). Mp. = 218–220 °C. MS (EI)  $[M]^+$ :  $m/z$  = 424. <sup>1</sup>H NMR (400 MHz, DMSO-*d*<sub>6</sub>) δ 8.51 (d,  $J$  = 2.6 Hz, 1H), 8.19 (s, 1H), 8.04 (d,  $J$  = 8.5 Hz, 1H), 7.71 (d,  $J$  = 7.9 Hz, 2H), 7.58 (d,  $J$  = 7.7 Hz, 1H), 7.47 (t,  $J$  = 4.4 Hz, 3H), 7.37 (s, 1H), 6.94 (d,  $J$  = 8.5 Hz, 1H), 5.71 (s, 1H), 3.91 (s, 1H), 1.81 (s, 1H), 0.83 (d,  $J$  = 8.0 Hz, 4H). <sup>13</sup>C NMR (101 MHz, DMSO-*d*<sub>6</sub>) δ 172.27, 163.67, 147.16, 145.27, 140.41, 138.08, 137.40, 135.63, 131.59, 129.84, 129.25, 127.25, 122.09, 120.45, 118.96, 116.09, 111.15, 53.81, 53.20, 15.07, 7.74.

#### 4.1.11. 3-(4-((4-(3-chlorophenyl)-1*H*-1,2,3-triazol-1-yl) methyl) phenyl)pyridine (**BD9**)

Mp. = 140–142 °C. MS (EI)  $[M]^+$ :  $m/z$  = 346. <sup>1</sup>H NMR (400 MHz, DMSO-*d*<sub>6</sub>) δ 8.90 (d,  $J$  = 1.9 Hz, 1H), 8.81 (s, 1H), 8.59 (dd,  $J$  = 4.8, 1.5 Hz, 1H), 8.08 (d,  $J$  = 8.0 Hz, 1H), 7.94 (s, 1H), 7.86 (d,  $J$  = 7.8 Hz, 1H), 7.78 (d,  $J$  = 8.3 Hz, 2H), 7.54–7.47 (m, 4H), 7.40 (dd,  $J$  = 7.6, 1.5 Hz, 1H), 5.74 (s, 2H). <sup>13</sup>C NMR (101 MHz, DMSO-*d*<sub>6</sub>) δ 149.16, 148.16, 145.86, 137.49, 136.22, 135.46, 134.63, 134.18, 133.22, 131.36, 129.28, 128.17, 127.85, 125.26, 124.38, 124.16, 122.89, 53.25.

#### 4.1.12. 3-(4-((4-(2-fluorophenyl)-1*H*-1,2,3-triazol-1-yl) methyl) phenyl)pyridine (**BD10**)

Mp. = 115–117 °C. MS (EI)  $[M]^+$ :  $m/z$  = 344. <sup>1</sup>H NMR (400 MHz, DMSO-*d*<sub>6</sub>) δ 8.89 (s, 1H), 8.63–8.54 (m, 2H), 8.17–8.11 (m, 1H), 8.07 (d,  $J$  = 8.1 Hz, 1H), 7.76 (d,  $J$  = 8.3 Hz, 2H), 7.49 (dd,  $J$  = 13.1, 5.9 Hz, 3H), 7.43–7.29 (m, 3H), 5.76 (s, 2H). <sup>13</sup>C NMR (101 MHz, DMSO-*d*<sub>6</sub>) δ 149.15, 148.16, 140.40, 137.42, 136.45, 135.49, 134.63, 130.25, 130.16, 129.24, 127.82, 125.46, 124.61, 124.49, 124.37, 116.62, 116.41, 53.00.

#### 4.1.13. 3-(4-((4-phenyl-1*H*-1,2,3-triazol-1-yl)methyl)phenyl) pyridine (**BD11**)

Mp. = 162–164 °C. MS (EI)  $[M]^+$ :  $m/z$  = 312. <sup>1</sup>H NMR (400 MHz, DMSO-*d*<sub>6</sub>) δ 8.90 (s, 1H), 8.70 (s, 1H), 8.58 (s, 1H), 8.08 (d,  $J$  = 8.1 Hz, 1H), 7.92–7.86 (m, 2H), 7.77 (d,  $J$  = 8.2 Hz, 2H), 7.52–7.42 (m, 5H), 7.34 (t,  $J$  = 7.4 Hz, 1H). <sup>13</sup>C NMR (101 MHz, DMSO-*d*<sub>6</sub>) δ 149.17, 148.18, 147.23, 137.45, 136.46, 135.51, 134.65, 131.15, 129.42, 129.22, 128.43, 127.86, 125.68, 124.40, 122.15, 53.17.

#### 4.1.14. 3-(4-((4-(*p*-tolyl)-1*H*-1,2,3-triazol-1-yl)methyl) phenyl) pyridine (**BD12**)

Mp. = 162–164 °C. MS (EI)  $[M]^+$ :  $m/z$  = 326. <sup>1</sup>H NMR (400 MHz, DMSO-*d*<sub>6</sub>) δ 8.90 (d,  $J$  = 2.1 Hz, 1H), 8.66–8.63 (m, 1H), 8.59 (d,  $J$  = 4.7 Hz, 1H), 8.08 (d,  $J$  = 8.1 Hz, 1H), 7.76 (t,  $J$  = 7.7 Hz, 4H), 7.49 (d,  $J$  = 8.3 Hz, 3H), 7.26 (d,  $J$  = 8.0 Hz, 2H), 5.71 (s, 2H), 2.33 (s, 3H). <sup>13</sup>C NMR (101 MHz, DMSO-*d*<sub>6</sub>) δ 149.18, 148.19, 147.29, 137.72, 137.44, 136.49, 135.52, 134.65, 129.97, 129.23, 128.39, 127.85, 125.62, 124.41, 121.71, 53.14, 21.34.

#### 4.1.15. 3-(4-((4-(*m*-tolyl)-1*H*-1,2,3-triazol-1-yl)methyl) phenyl) pyridine (**BD13**)

Mp. = 165–167 °C. MS (EI)  $[M]^+$ :  $m/z$  = 326. <sup>1</sup>H NMR (400 MHz, DMSO-*d*<sub>6</sub>) δ 8.81 (d,  $J$  = 1.9 Hz, 1H), 7.61 (s, 2H), 7.57 (d,  $J$  = 7.8 Hz, 1H), 7.45–7.38 (m, 1H), 7.25 (t,  $J$  = 7.6 Hz, 1H). <sup>13</sup>C NMR (101 MHz, DMSO-*d*<sub>6</sub>) δ 149.18, 148.19, 147.32, 138.56, 137.46, 136.46, 135.52, 134.66, 131.07, 129.32, 129.26, 129.08, 127.86, 126.25, 124.41, 122.83, 122.08, 53.16, 21.55.

#### 4.1.16. 3-(4-((4-(4-(trifluoromethyl)phenyl)-1*H*-1,2,3-triazol-1-yl) methyl)phenyl)pyridine (**BD14**)

Mp. = 173–175 °C. MS (EI)  $[M]^+$ :  $m/z$  = 380. <sup>1</sup>H NMR (400 MHz, DMSO-*d*<sub>6</sub>) δ 8.90 (d,  $J$  = 2.0 Hz, 2H), 8.58 (d,  $J$  = 6.0 Hz, 1H), 8.09 (t,  $J$  = 8.1 Hz, 3H), 7.80 (dd,  $J$  = 18.0, 8.3 Hz, 4H), 7.54–7.47 (m, 3H), 5.76 (s, 2H). <sup>13</sup>C NMR (101 MHz, DMSO-*d*<sub>6</sub>) δ 149.19, 148.19, 145.86, 137.54, 136.23, 135.49, 135.12, 134.65, 129.32, 127.88, 126.43, 126.39, 126.21, 126.11, 124.39, 123.44, 53.30.

#### 4.1.17. 3-(4-((4-(3-(trifluoromethyl)phenyl)-1*H*-1,2,3-triazol-1-yl) methyl)phenyl)Pyridine (**BD15**)

Mp. = 110–112 °C. MS (EI)  $[M]^+$ :  $m/z$  = 380. <sup>1</sup>H NMR (400 MHz, DMSO-*d*<sub>6</sub>) δ 8.90 (s, 2H), 8.64–8.56 (m, 1H), 8.21 (s, 2H), 8.08 (d,  $J$  = 8.0 Hz, 1H), 7.78 (d,  $J$  = 8.2 Hz, 2H), 7.71 (d,  $J$  = 5.1 Hz, 2H), 7.54–7.45 (m, 3H), 5.75 (s, 2H). <sup>13</sup>C NMR (101 MHz, DMSO-*d*<sub>6</sub>) δ 149.20, 148.18, 145.86, 137.54, 136.22, 135.49, 134.66, 132.22, 130.65, 129.46, 129.34, 127.89, 124.93, 124.89, 124.41, 123.15, 122.04, 122.01, 53.32.

#### 4.1.18. 3-(1-(4-(pyridin-3-yl)benzyl)-1*H*-1,2,3-triazol-4-yl) aniline (**BD16**)

Mp. = 189–191 °C. MS (EI)  $[M]^+$ :  $m/z$  = 327. <sup>1</sup>H NMR (400 MHz, DMSO-*d*<sub>6</sub>) δ 8.90 (s, 1H), 8.59 (s, 1H), 8.52 (s, 1H), 8.08 (d,  $J$  = 8.1 Hz, 1H), 7.76 (d,  $J$  = 8.2 Hz, 2H), 7.49 (t,  $J$  = 7.0 Hz, 3H), 7.14–7.03 (m, 2H), 6.94 (d,  $J$  = 7.6 Hz, 1H), 6.52 (d,  $J$  = 9.3 Hz, 1H), 5.69 (s, 2H), 5.18 (s, 2H). <sup>13</sup>C NMR (101 MHz, DMSO-*d*<sub>6</sub>) δ 149.57, 149.17, 148.18, 147.89, 137.41, 136.57, 135.53, 134.65, 131.60, 129.87, 129.22, 127.84,

124.41, 121.69, 114.12, 113.51, 110.94, 53.06, 39.79.

#### 4.2. RTK inhibitory activity assay

The in vitro RTK inhibition assays against VEGFR-2, Tie-2 and EphB4 of all the title compounds were detected using ADP-Glo™ kinase assay kit (Promega, Madison) with sorafenib as the positive control. The kinase assay was performed in a reaction mixture of 5  $\mu$ L final volume. General procedure is as follows: for VEGFR-2 assay, the tyrosine kinase (0.6 ng/mL) was incubated with substrates (0.2 mg/mL), test title compound ( $1.2 \times 10^{-4} \sim 12 \mu$ M) and ATP (50  $\mu$ M) in a final buffer of Tris 40 mM, MgCl<sub>2</sub> 10 mM, BSA 0.1 mg/mL, DTT 1 mM in 384-well plate with the total volume of 5  $\mu$ L. The plate was incubated at 30 °C for 1 h. After the plate was cooled at room temperature for 5 min, 5  $\mu$ L of ADP-Glo reagent was added into each well to stop the kinase reaction and consume the remaining ATP within 40 min. At the end, 10  $\mu$ L kinase detection reagent was added into the well and incubated for 30 min to produce a luminescence signal. As for Tie-2 and EphB4 assays, the kinases (2.4 ng/mL) were incubated with substrates (0.2 mg/mL), test title compound ( $1.2 \times 10^{-4} \sim 12 \mu$ M) and ATP (50  $\mu$ M) in a final buffer of Tris 40 mM, MgCl<sub>2</sub> 10 mM, BSA 0.1 mg/mL, DTT 1 mM in 384-well plate with the total volume of 5  $\mu$ L. The plate was incubated at 30 °C for 4 h. After the plate was cooled at room temperature for 5 min, 5  $\mu$ L of ADP-Glo reagent was added into each well to stop the kinase reaction and consume the remaining ATP within 1 h. At the end, 10  $\mu$ L kinase detection reagent was added into the well and incubated for 30 min to produce a luminescence signal. The luminescence was read by VICTOR-X multi-label plate reader.

#### 4.3. Antiproliferative activity against human vascular endothelial cell (EA.hy926)

The viability of HUVEC (EA.hy926) was assessed using the cell counting kit-8 (CCK-8, Sigma, USA) assay according to the manufacturer's instruction. Briefly, EA.hy926 cells were harvested and plated in a 96-well plate at the density of  $1 \times 10^5$  cells for each well, and cultured in DMEM medium with 10% FBS in humidified 5% CO<sub>2</sub>. After incubation at 37 °C for 48 h, the cells were treated with tested compounds at serial diluted concentration for 24 h subsequently, premixed CCK-8 and medium (10  $\mu$ L) were added into the 96-well plate to monitor cell viability and were incubated at 37 °C for 2 h. The number of viable cells was assessed by measurement of absorbance at 450 nm by a microplate reader. The viability rate was calculated as experimental OD value/control OD value. The IC<sub>50</sub> values were calculated according to inhibition ratios.

#### 4.4. Molecular docking study

Surflex-Dock module of Sybyl-X (version 2.0, Tripos Inc, St. Louis, MO) was used in docking study. The crystal structures of VEGFR-2 (PDB ID: 4ASD), TIE-2 (PDB ID: 2P4I) and EphB4 (PDB ID: 2X9F) were downloaded from the Protein Bank. Prior to docking, the ligand was extracted from complex structure and was regarded as the reference molecule. Waters and some other small molecules were removed. All the hydrogen atoms and AMBER7 FF99 charges were added. Compound **BD7** was generated and optimized using Powell's method with Tripos force field with convergence criterion set at 0.05 kcal/( $\text{\AA}$ mol). Then Gasteiger-Hückel charges were assigned to the small molecule. The residues in 5.0  $\text{\AA}$  around the ligand were considered as active site. The optimized confirmation of BD7 was then docked into the active site of protein. Other parameters were kept as default.

#### 4.5. Protein structure alignment

Align structure module of Sybyl-X (version 2.0, Tripos Inc, St. Louis, MO) was used in protein homology study. The crystal structures of VEGFR-2 (PDB ID: 4ASD), Tie-2 (PDB ID: 2P4I) and EphB4 (PDB ID: 2X9F) were downloaded from the Protein Bank. First, protein preparation was performed as follows: removing waters and other small molecules, repairing sidechain, and adding hydrogen atoms. The fixed structure was saved as mol file. Second, either two structure of VEGFR-2, TIE-2 and EphB4 were imported, one as reference structure and the other one as movable structure. Then alignment was performed with parameters as default. Finally, the overlay results was shown on the window, and the identity and RMSD results was calculated in the command console automatically. The overlaid structure was visualized by PyMOL.

#### Acknowledgments

This work was supported by the National Natural Science Foundation of China (NSFC, Grant No. 81573285 and No. 81602965), the Natural Science Basic Research Plan in Shaanxi Province of China (Program No. 2018JM7071 and No. 2017JQ8002), and the Fundamental Research Funds for the Central Universities (2015qngz13).

#### Appendix A. Supplementary data

Supplementary data to this article can be found online at <https://doi.org/10.1016/j.ejmech.2018.11.042>.

#### References

- [1] J.R. Nathan, G. Lakshmanan, F.M. Michael, P. Seppan, M. Ragunathan, Expression of adenosine receptors and vegf during angiogenesis and its inhibition by pentoxifylline-A study using zebrafish model, *Biomed. Pharmacother.* 84 (2016) 1406–1418.
- [2] Z. Lin, Q. Zhang, W. Luo, Angiogenesis inhibitors as therapeutic agents in cancer: challenges and future directions, *Eur. J. Pharmacol.* 793 (2016) 76–81.
- [3] G. Aprile, M. Macerelli, F. Giuliani, Regorafenib for gastrointestinal malignancies: from preclinical data to clinical results of a novel multi-target inhibitor, *BioDrugs* 27 (2013) 213–224.
- [4] L.L. Jardim, D.R. Rios, L.O. Perucci, L.P. de Sousa, K.B. Gomes, L.M. Dusse, Is the imbalance between pro-angiogenic and anti-angiogenic factors associated with preeclampsia? *Clin. Chim. Acta* 447 (2015) 34–38.
- [5] S.P. Herbert, D.Y. Stainier, Molecular control of endothelial cell behavior during blood vessel morphogenesis, *Nat. Rev. Mol. Cell Biol.* 12 (2011) 551–564.
- [6] G. Martiny-Baron, P. Holzer, E. Billy, C. Schnell, J. Brueggen, M. Ferretti, N. Schmiedeberg, J.M. Wood, P. Furet, P. Imbach, The small molecule specific EphB4 kinase inhibitor NVP-BHG712 inhibits VEGF driven angiogenesis, *Angiogenesis* 13 (2010) 259–267.
- [7] S.M. Weis, D.A. Cheresh, Tumor angiogenesis: molecular pathways and therapeutic targets, *Nat. Med.* 17 (2011) 1359–1370.
- [8] D. Bouis, Y. Kusumanto, C. Meijer, N.H. Mulder, G.A. Hospers, A review on pro and anti-angiogenic factors as targets of clinical intervention, *Pharmacol. Res.* 53 (2006) 89–103.
- [9] J.P. Himanen, K.R. Rajashankar, M. Lackmann, C.A. Cowan, M. Henkemeyer, D.B. Nikolov, Crystal structure of an Eph receptor-ephrin complex, *Nature* 414 (2001) 933–938.
- [10] D. Hanahan, J. Folkman, Patterns and emerging mechanisms of the angiogenic switch during tumorigenesis, *Cell* 86 (1996) 353–364.
- [11] J.S. Papadopoulos, R. Agarwala, COBALT: constraint-based alignment tool for multiple protein sequences, *Bioinformatics* 23 (2007) 1073–1079.
- [12] X. Robert, P. Gouet, Deciphering key features in protein structures with the new END script server, *Nucleic Acids Res.* 42 (2014) W320–W324.
- [13] Y. Shan, H. Gao, X. Shao, J. Wang, X. Pan, J. Zhang, Discovery of novel VEGFR-2 inhibitors. Part 5: exploration of diverse hinge-binding fragments via core refining approach, *Eur. J. Med. Chem.* 103 (2015) 80–90.
- [14] P. Su, J. Wang, Y. Shi, X. Pan, R. Shao, J. Zhang, Discovery of biphenyl-aryl ureas as novel VEGFR-2 inhibitors. Part 4: exploration of diverse hinge-binding fragments, *Bioorg. Med. Chem.* 23 (2015) 3228–3236.
- [15] H. Gao, P. Su, Y. Shi, X. Shen, Y. Zhang, J. Dong, J. Zhang, Discovery of novel VEGFR-2 inhibitors. Part II: biphenyl urea incorporated with salicylaldehyde, *Eur. J. Med. Chem.* 90 (2015) 232–240.
- [16] B. Dai, J. Qi, R. Liu, J. Zhang, Y. Zhan, Y. Zhang, A novel compound T7 (N-[4-

- [(1E)-N-hydroxyethanimidoyl]-3',5,6-trimethoxybiphenyl-3-yl]-N'-[4-(3-morpholin-4-ylpropoxy)phenyl] urea) screened by tissue angiogenesis model and its activity evaluation on anti-angiogenesis, *Phytomedicine* 21 (2014) 1675–1683.
- [17] X. Pan, F. Wang, Y. Zhang, H. Gao, Z. Hu, S. Wang, J. Zhang, Design, synthesis and biological activities of Nilotinib derivatives as antitumor agents, *Bioorg. Med. Chem.* 21 (2013) 2527–2534.
- [18] D. Rodríguez-Hernández, L.C.A. Barbosa, A.J. Demuner, A. Nain-Perez, S.R. Ferreira, R.T. Fujiwara, R.M. de Almeida, L. Heller, R. Csuk, Leishmanicidal and cytotoxic activity of hederagenin-bistriazolyl derivatives, *Eur. J. Med. Chem.* 140 (2017), 624–6635.
- [19] K. Arunrungvichian, V.V. Fokin, O. Vajragupta, P. Taylor, Selectivity optimization of substituted 1,2,3-triazoles as  $\alpha 7$  nicotinic acetylcholine receptor agonists, *ACS Chem. Neurosci.* 6 (2015) 1317–1330.
- [20] X. Pan, J. Dong, Y. Shi, R. Shao, F. Wei, J. Wang, J. Zhang, Discovery of novel Bcr-Abl inhibitors with diacylated piperazine as the flexible linker, *Org. Biomol. Chem.* 13 (2015) 7050–7066.
- [21] H. Zegzouti, M. Zdanovskaia, K. Hsiao, S.A. Goueli, ADP-Glo: a Bioluminescent and homogeneous ADP monitoring assay for kinases, *Assay Drug Dev. Technol.* 7 (2009) 560–572.
- [22] S. Wang, J. Chen, Y. Fu, X. Chen, Promotion of astragaloside iv for EA-hy926 cell proliferation and angiogenic activity via ERK1/2 pathway, *J. Nanosci. Nanotechnol.* 15 (2015) 4239–4244.
- [23] J. Zhang, Y. Shan, X. Pan, C. Wang, W. Xu, L. He, Molecular docking, 3D-QSAR studies, and in silico ADME prediction of p-aminosalicylic acid derivatives as neuraminidase inhibitors, *Chem. Biol. Drug Des.* 78 (2011) 709–717.